Title: Electrophysical properties of the multicomponent PBZT-type ceramics doped by Sn4+

Author: Dariusz Bochenek, Przemysław Niemiec, Ryszard Skulski, Małgorzata Adamczyk-Habrajska, Dagmara Brzezińska

CrossMark

Electrophysical properties of the multicomponent PBZT-type ceramics doped by Sn^{4+}

Dariusz Bochenek[1] · Przemysław Niemiec[1] · Ryszard Skulski[1] · Małgorzata Adamczyk[1] · Dagmara Brzezińska[1]

Abstract

In the work, the multicomponent $Pb_{0.75}Ba_{0.25}(Zr_{0.65}Ti_{0.35})_{1-a}Sn_aO_3$ (PBZT/Sn) ceramics were obtained with various tin amounts (a from the range of 0.0 to 0.1). The densification of the PBZT/Sn ceramic samples was performed using pressureless sintering method. The effect of SnO_2 content on the crystal structure of PBZT/Sn ceramics, microstructure, DC electrical conductivity and electrophysical properties (including dielectric and ferroelectric testes), were investigated. The PBZT/Sn ceramic samples exhibit high values of dielectric permittivity at the temperature of ferro-paraelectric phase transition and show the relaxor character of phase transition. Excessive SnO_2 contents doping of the PBZT/Sn materials (already for $a = 0.1$) might lead to lattice stress and structure defects, which successively leads to the deterioration of ferroelectric and dielectric properties of the ceramic samples. The presented research shows that the addition of SnO_2 to the base PBZT compound (in the proper proportion) gives an additional possibility of influencing the parameters essential for practical applications, from the areas of micromechatronics and microelectronics.

Keywords Perovskite · Dielectric properties · Relaxors · PZT-type ceramics

1 Introduction

Ferroelectric PZT-type materials belong to the most renowned families of functional materials and are at the peak of research, as well as have attracted the attention of technologists and researchers due to their excellent piezoelectric, pyroelectric and non-linear optical properties [1–3]. Piezomaterials have broad applications in electromechanical and electroacoustic transducers, bandwidth filters, transformers, frequency stabilized resonators, hydroacoustic applications and semiconductor materials for special purposes [4]. Ferroelectric materials with diffuse phase transition provide the basic requirements to obtain ceramic materials with high dielectric permittivity and low temperature coefficients, necessary for multilayer ceramic capacitor applications [5]. The Ba-modified $Pb(Zr_{1-x}Ti_x)O_3$ (PBZT) ceramic composition remains for many years an interesting ferroelectric material, as a result of interesting physical properties (very high value of electrical permittivity weakly

depending on temperature) [6–10]. The PBZT ceramic materials with ferroelectric relaxor properties have been reported as a good candidate for microelectronic applications [11–13]. Examples of such applications can be electrostrictive actuators due to large electrostrictive strain, transducers, sensors, etc. [14–16]. The phase diagram of PBZT as a function of barium content has been presented for the first time in 1959 [14]. A typical property for ferroelectric relaxors is a broad maximum of dielectric permittivity depending insignificantly on temperature, narrow hysteresis loop slowly diminishing with an increasing temperature, and the lack of phase transition in a macroscopic scale [17]. In a $Pb_{1-y}Ba_yZr_{0.65}Ti_{0.35}O_3$ ceramics with $y < 0.40$, the normal ferroelectric behavior and a rhombohedral structure has been observed [14], which can be explained by a less deformed octahedral environment of the Zr/Ti cations [18–20]. From a wide application point of view, the PBZT compound should be modified in order to be employed in practical device elements [21–24]. In this type of compounds an important feature is the possibility of controlling parameters, as a result of isovalent or heterovalent substitutions by other ions in A or B positions of the perovskite structures [25, 26].

In our previous work [7], we investigated PBZT doped by Sn^{4+} i.e. the solid solution of $Pb_{0.75}Ba_{0.25}(Zr_{0.65}Ti_{0.35})_{1-a}Sn_aO_3$ (PBZT/Sn) with rhombohedral structure (in the ceramic form), with various amounts of tin (a from the range

✉ Dariusz Bochenek
dariusz.bochenek@us.edu.pl

[1] Faculty of Computer Science and Material Science, Institute of Technology and Mechatronics, University of Silesia in Katowice, 12, Żytnia St., 41–200, Sosnowiec, Poland

0.0 to 0.1) sintered at 1250 °C/4 h. The introduction of the tin admixture into the base composition was intended, inter alia, to reduce the width of the hysteresis loop while maintaining optimal electric parameters of the obtained materials. In addition to the above, the selection criteria for tin admixture of the PBZT composition have taken into account also the following arguments: the polarizability of the tin cation (in common valence state) at the level of 2.83 Å^3 (the induced ionic dipole moment is large if the polarizability of the ion is large [27]), not toxic, possible candidates for B position in perovskite-type structure, as well as similar ionic radius of occupied cations. Introduction of the Sn^{4+} ion into the B-position of the perovskite structure causes changes of parameters important for applications in devices, such as actuators which convert energy from one form to another and pulse capacitors which accumulate charges. The results of the research presented in the paper were compared also with the previous work [28], in which the authors obtained this material using different technological conditions (higher sintering temperature 1300 °C and longer sintering time 5 h). In the present work, we continue the investigations from our works [7, 28].

2 Experimental details

2.1 Preparation of the ceramic materials

In the technological process of the PBZT/Sn ceramic samples the simple oxides i.e.: PbO (99.9%, POCH), ZrO$_2$ (99.5%, Aldrich), TiO$_2$ (99.9%, Merck), SnO$_2$ (99.9%, Aldrich) and BaCO$_3$ carbonate (99.99%, POCH) have been used as a staring components. The starting ingredients were mixed in a FRITSCH planetary ball mill for 15 h with the usage of the wet method in ethyl alcohol. Successively, the mixtures of powders were calcined using the following conditions: 850 °C/3 h. In the next step, the calcined powders were additionally pulverized and pressed into disks. The densification of the PBZT/Sn samples was performed by pressureless sintering method using the following conditions: 1250 °C/4 h. The final steps of technology were grinding, polishing, annealing at following condition 700 °C/15 min. (removing mechanical stresses) and for electrical testing putting silver paste electrodes onto both surfaces of the samples.

The six multicomponent PBZT/Sn ceramic compositions with the following chemical formulas: (i) Pb$_{0.75}$Ba$_{0.25}$(Zr$_{0.65}$Ti$_{0.35}$)O$_3$ (P-1), (ii) Pb$_{0.75}$Ba$_{0.25}$(Zr$_{0.65}$Ti$_{0.35}$)$_{0.98}$Sn$_{0.02}$O$_3$ (P-2), (iii) Pb$_{0.75}$Ba$_{0.25}$(Zr$_{0.65}$Ti$_{0.35}$)$_{0.96}$Sn$_{0.04}$O$_3$ (P-3), (iv) Pb$_{0.75}$Ba$_{0.25}$(Zr$_{0.65}$Ti$_{0.35}$)$_{0.94}$Sn$_{0.06}$O$_3$ (P-4), (v) Pb$_{0.75}$Ba$_{0.25}$(Zr$_{0.65}$Ti$_{0.35}$)$_{0.92}$Sn$_{0.08}$O$_3$ (P-5), (vi) Pb$_{0.75}$Ba$_{0.25}$(Zr$_{0.65}$Ti$_{0.35}$)$_{0.90}$Sn$_{0.10}$O$_3$ (P-6) were obtained and investigated.

2.2 Characterization

The X-ray investigations of the crystal structure at room temperature (RT) have been made using a diffractometer Phillips X'Pert APD (Cu-Kα radiation). Microstructure and EDS (Energy Dispersive Spectrometry) measurements were carried out using a JEOL JSM-7100 TTL LV Field Emission Scanning Electron Microscope. Dielectric measurements were performed using a QuadTech 1920 LCR meter during heating cycle (at frequencies from 20 Hz to 20 kHz), in the temperature range of 20 °C to 230 °C. Ferroelectric investigations (ferroelectric hysteresis P–E loops) were made using a Sawyer-Tower circuit and a high voltage amplifier (Matsusada Inc. HEOPS-5B6 Precision), while electromechanical measurements were carried out using an optical displacement meter (Philtec Inc., D63) and a high voltage amplifier (HEOPS-5B6). The data were stored on a computer disc using an A/D, D/A transducer card and the LabView computer program. DC electrical conductivity has been measured using a Keithley 6517B electrometer (high resistance meter) in the temperature range of 25 °C to 450 °C.

3 Results and discussion

3.1 X-ray diffraction analysis

The results of XRD investigations for all PBZT/Sn materials are presented in Fig. 1. At room temperature, XRD patterns exhibit maxima belonging to the perovskite phase. It suggests that in the obtained PBZT/Sn ceramic samples tin incorporates into B-positions of the crystal lattice. As a result, additional phases are not observed, e.g., pyrochlore phase. The crystal structure measurements show that all PBZT/Sn samples have pseudo-cubic structures, typical for relaxor materials (selected enlarged region in Fig. 1 - the maxima do not consist of two or more components) [29]. The Goldschmidt tolerance factor t is used to demonstrate the degree of distortion of the ABO$_3$ perovskite structure and will be calculated according to formula (1):

$$t = \frac{0.75R_{Pb} + 0.25R_{Ba} + R_O}{\sqrt{2}\left[(0.65R_{Zr} + 0.35R_{Ti})_{1-a} + aR_{Sn} + R_O\right]} \quad (1)$$

where: R_A, R_B are the ionic radii of the A-site and B-site cation, respectively, R_O is the ionic radii of the oxygen anion. The tolerance factor of 1.0 indicates the formation of an ideal type perovskite with a cubic crystal structure. If the values for t are between 1.0 and 0.9, perovskites with a cubic crystal structure are formed predominantly, while when the t is lower (between 0.80 and 0.89), distorted perovskite structures with orthorhombic, tetragonal, or rhombohedral crystal structures are more probable to be

Fig. 1 XRD Patterns at room temperature and selected enlarged region (from 43° to 46°) of the PBZT/Sn ceramics
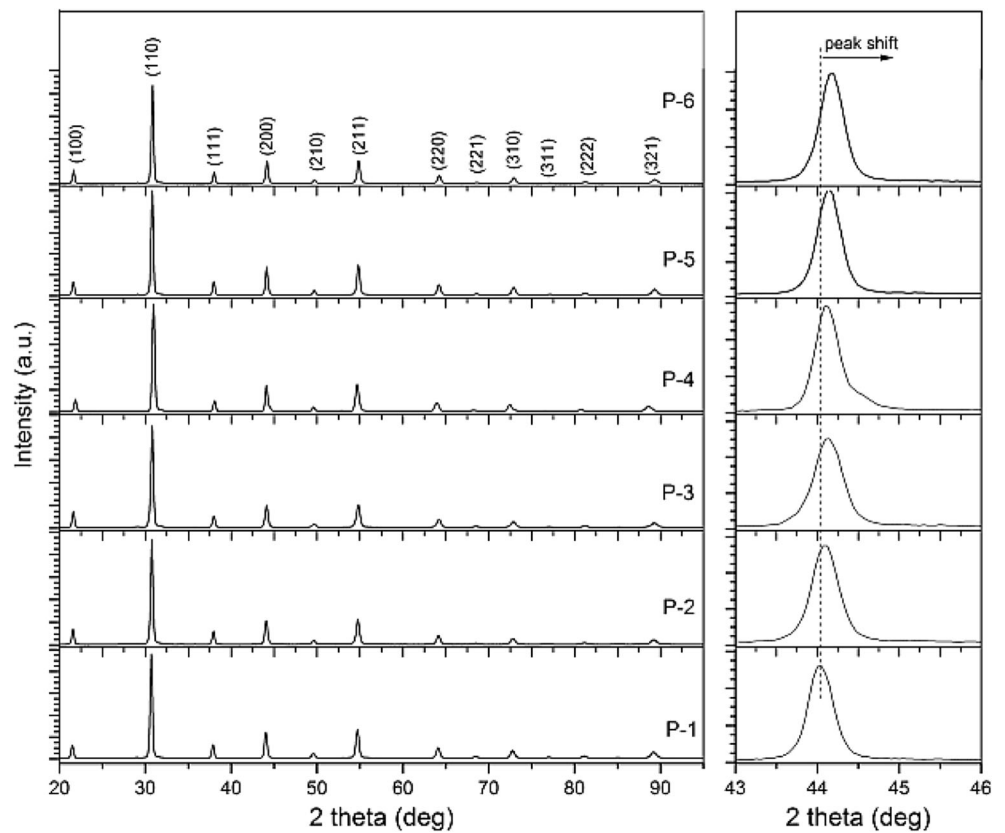
formed [30]. When $t < 0.8$ or $t > 1.0$, the A cation is too small or too large, respectively, for the formation of a perovskite structure [31]. The calculated values of tolerance factor t are listed in Table 1 and confirm that the material has a pseudo-cubic structure.

From selected enlarged region in Fig. 1, it is seen that the diffraction peaks shift towards a higher angle with increasing SnO_2 contents. It can be a result of the substitution of the Zr^{4+} ions (0.072 nm ionic radius) and/or Ti^{4+} (0.061 nm ionic radius) by the Sn^{4+} (0.069 nm ionic radius) [32]. It is seen that

Table 1 Electrophysical parameters of the PBZT/Sn ceramics

	P-1	P-2	P-3	P-4	P-5	P-6
a_0 (Å)	4.110(4)	4.103(3)	4.101(7)	4.100(5)	4.100(3)	4.097(3)
cell vol (Å^c)	69.450	69.090	69.007	68.947	68. 938	68.788
t	0.9887	0.9886	0.9885	0.9884	0.9883	0.9882
ρ (g/cm^c)	6.95	7.01	7.09	6.98	7.11	6.56
T_m (°C) [a]	147	140	138	123	108	93
ε_r [a]	3712	4038	4042	4876	5144	6352
ε_{max} [a]	11,093	10,307	10,218	11,224	10,400	10,505
tanδ at RT [a]	0.058	0.060	0.056	0.068	0.069	0.086
tanδ at T_m [a]	0.010	0.017	0.020	0.028	0.029	0.033
E_{Act} in I (eV)	0.313	0.164	0.274	0.174	0.201	0.134
E_{Act} in II (eV)	0.748	0.693	0.768	0.669	0.649	0.368
E_C (kV/mm) [b]	0.58	0.51	0.51	0.45	0.31	0.50
P_R (μC/cm) [b]	19.88	18.86	18.07	10.22	6.18	7.28
P_S (μC/cm) [b]	23.97	23.84	24.46	23.67	21.38	18.43
a_{rec} [b]	0.76	0.72	0.74	0.69	0.29	0.39
d_{33}^* (pm/V) [c]	729	560	467	440	433	427

[a] result for 1 kHz

[b] result for 1 Hz, at 30 °C

[c] calculeted from formula (9) for $E_{max} = 3.75$ kV/mm

t – tolerance factor, RT – room temperature, T_m – temperature at which there is maximum value of the dielectric permittivity

Sn^{4+} ionic radius is similar to Zr^{4+} and Ti^{4+}. Since Zr^{4+} ions are dominating in B-positions substitution Zr^{4+}/Sn^{4+} leads to the decrease of the elementary cell parameter. Ionic radii have been calculated taking into account the degree of oxidation and the coordination number for perovskite structure A = 12 and B = 6 (according Shannon-Prewitt).

The parameters of the pseudo-cubic (distorted cubic) unit cell for all obtained samples were calculated and presented in Table 1. The maximum value of elementary cell parameter is observed for the P-1 sample. With increasing amount of Sn^{4+} in based composition, linear decrease of the elementary cell parameter is observed, which is consistent with the XRD results.
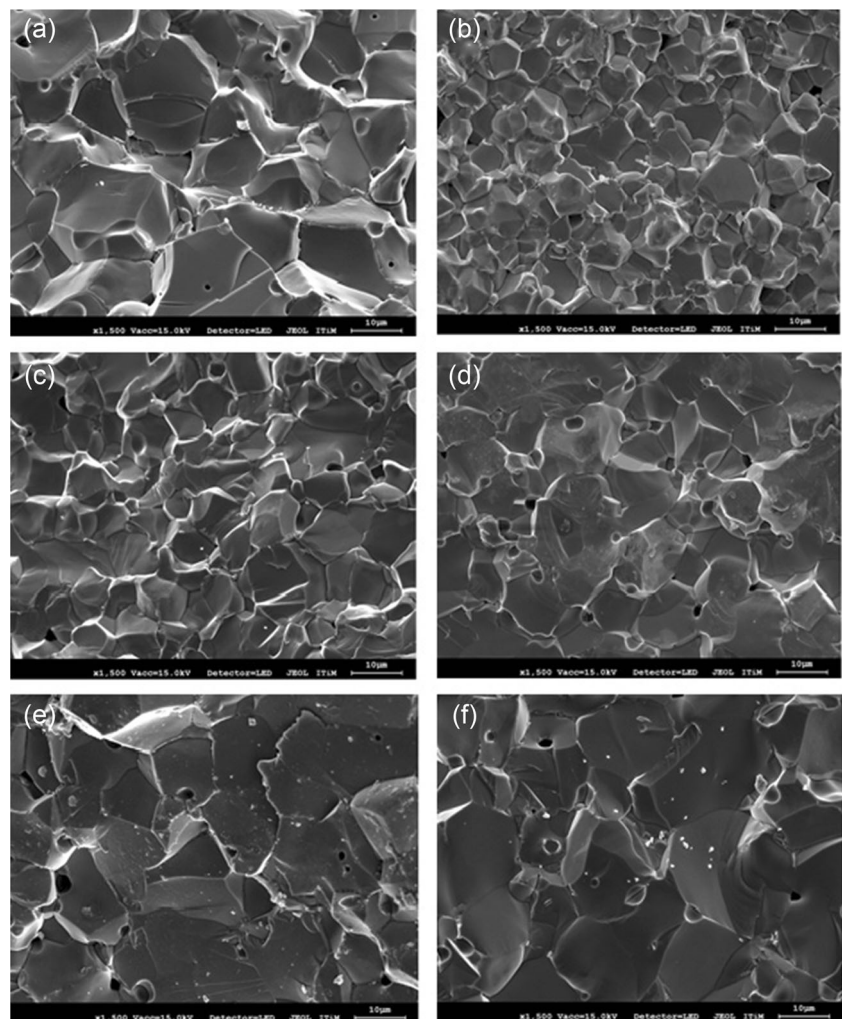
3.2 Microstructural testes

Not clear a trend is observed for the change of density with the increase of the Sn^{4+} admixture of the PBZT/Sn (Table 1). In the case of the P-1 and P-6 samples, the density is the smallest. One of the reasons of the reduction of density of the ceramic samples is the increase in the average grains size. Ceramic materials with large

grains are characterized by the presence of closed pores in the entire volume of the sample which decreases a total density.

For SEM testing, the ceramic samples were fractured, and on the examined surfaces (area of the fractured samples) a thin layer of gold was spread. The images of microstructures of the ceramic samples with different amounts of Sn^{4+} are shown in Fig. 2. The results show that all the samples featured have a dense packed microstructure and the grain boundaries are clear with few pores. The P-1 ceramic sample (without Sn^{4+} admixture) has a microstructure with large and mostly properly grown grains, but with a considerable heterogeneity of them. The grain boundaries of the P-1 sample have an unregulated and shapeless appearance.

The microstructure of the P-2 sample (with the least amount of tin) is fine-grained, with small and large grains. The fine grains do not reveal correct crystallization. Further increase of tin admixture amount in the basic PBZT/Sn composition increases the average size of grains. The grain boundaries become longitudinal and expressive. For the P-3 and P-4 samples, the highest grain

Fig. 2 SEM images of the PBZT/Sn materials (surfaces of fractured samples): (**a**) P-1, (**b**) P-2, (**c**) P-3, (**d**) P-4, (**e**) P-5, (**f**) P-6

Fig. 3 The EDS tests of the PBZT/Sn ceramics (with random microstructure)
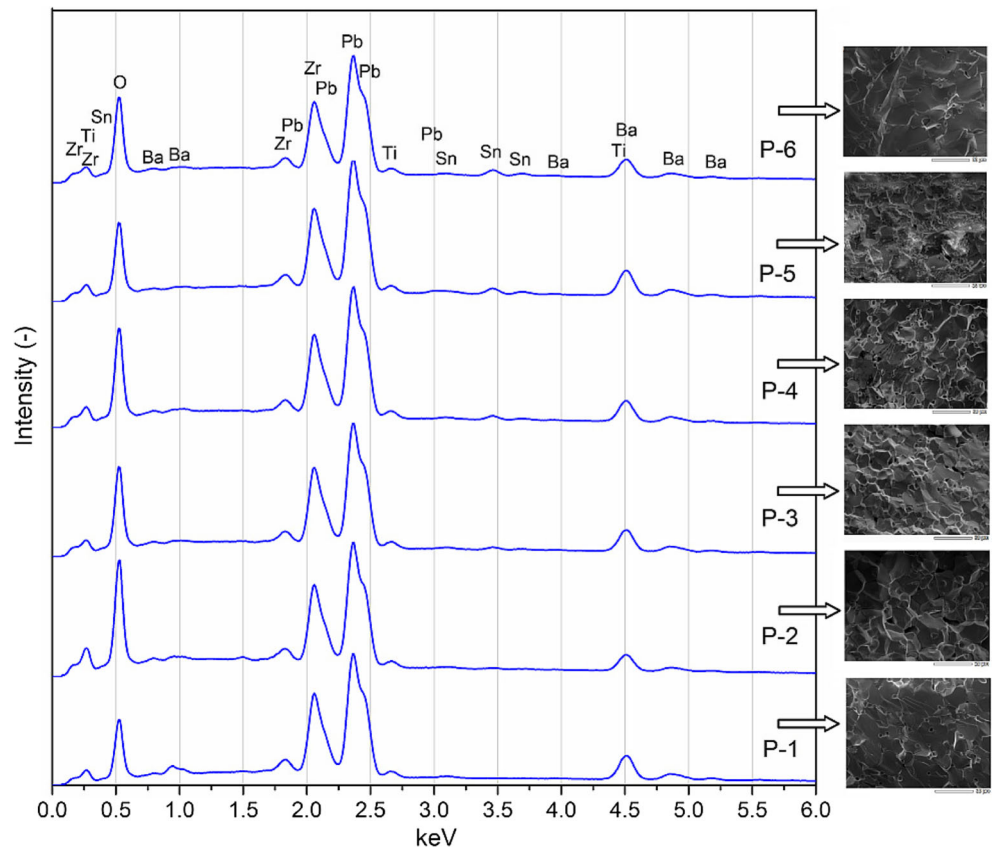
homogeneity is observed. For all the PBZT/Sn compositions, the fracture of samples is observed mainly through the grain boundaries, and to a lesser extent through grains. It indicates a higher strength inside the grains in comparison with their borders.

Chemical composition has been investigated using the EDS technique. The EDS analysis (Fig. 3) showed a visible increase in the amount of tin (SnL line - 3.46 kV) in the microstructure of the doped ceramic samples with Sn^{4+} admixture (a from 0.02 to 0.10). Research confirmed the qualitative composition of the obtained PBZT/Sn samples without the presence of foreign elements. In Table 2 the percentage of the individual components of the PBZT/Sn compositions were given. For all the PBZT/Sn ceramic samples, barium, zirconium and tin deficiency is observed, compared to theoretical calculations. At the same time, titanium and lead excesses are observed. All of the presented deviations from the initial composition are within an acceptable range.

3.3 DC electrical conductivity measurements

The motion of charges in the dielectric (ferroelectric) materials give rise to the conduction current and additionally polarize the dielectric, therefore tests of electrical conductivity in these materials are very important, inasmuch as dielectric, piezoelectric and pyroelectric properties depend on it. The results of investigations of DC electrical

Table 2 Theoretical and experimental percentages of elements (expressed as oxides) of PBZT/Sn ceramics

	P-1		P-2		P-3		P-4		P-5		P-6	
	th. (%)	ex. (%)	th. (%)	ex. (%)	th. (%)	ex. (%)	th. (%)	ex. (%)	th. (%)	ex. (%)	th. (%)	ex. (%)
PbO	53.35	55.8	53.2	55.29	53.06	55.7	52.92	55.07	52.78	54.46	52.63	53.73
BaO	12.22	10.52	12.18	10.94	12.15	11.35	12.12	11.32	12.08	11.25	12.05	11.17
ZrO_2	25.53	24.48	24.95	23.82	24.37	22.13	23.8	22.12	23.23	22.13	22.67	22.24
TiO_2	8.9	9.2	8.71	9.12	8.51	9.11	8.31	8.76	8.11	8.41	7.91	8.25
SnO_2	–	–	0.96	0.83	1.91	1.71	2.85	2.73	3.8	3.75	4.74	4.61

th. theoretical calculation; *ex.* expermental results
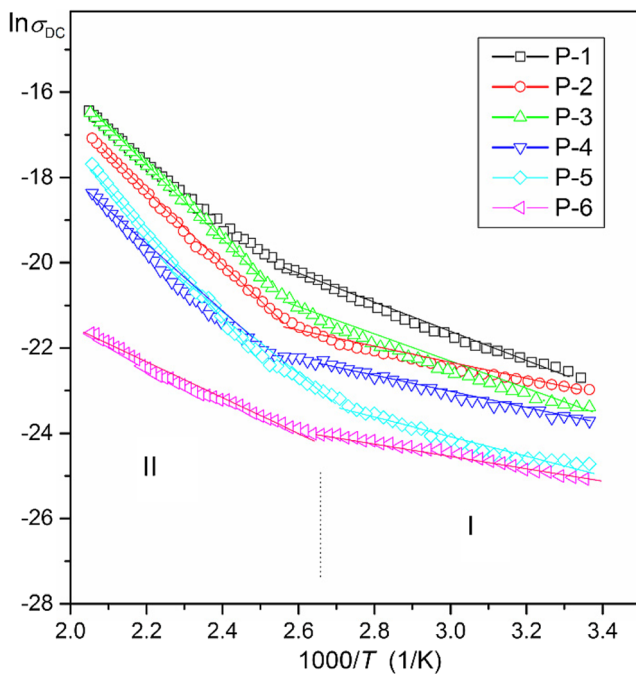
Fig. 4 The $\ln\sigma_{DC}(1000/T)$ of the PBZT/Sn ceramics

conductivity for all ceramic samples are presented in Fig. 4. The $\ln\sigma_{DC}(1000/T)$ plots for doped compositions have a similar character (except undoped P-1 sample).

On the basis of the Arrhenius formula (2), the activation energy value of the dielectric relaxation process can be calculated. Activation energy value was calculated from the slope of the linear portion of $\ln\sigma_{DC}(1000/T)$ plot.

$$\sigma_{DC} = \sigma_0 e^{-\frac{E_{Act}}{k_B T}} \tag{2}$$

where: σ_0 – pre-exponential factor, k_B – Boltzmann constant, E_{Act} – activation energy, T – absolute temperature.

There are two regions with a different slope of curves (i.e. with different values of activation energy – Table 1). The first range (I) concerns the area from the ferroelectric phase, whereas the second one (II) – the area from the paraelectric phase. Due to the difference in conductivity mechanism, different activation energy is observed in different temperature region. Like most materials with perovskite structure, also for the PBZT/Sn ceramics at lower temperatures (below ferroelectric-paraelectric phase transition) the value of activation energy is lower than above phase transition temperature [33]. In the first range the E_{Act} is 0.313 eV, 0.164 eV, 0.274 eV, 0.174 eV, 0.201 eV, 0.134 eV, while in the second range the E_{Act} is 0.748 eV, 0.693 eV, 0.768 eV, 0.669 eV, 0.649 eV, 0.368 eV for P-1, P-2, P-3, P-4, P-6 and P-6 samples, respectively. At higher temperatures, the conductivity vs. temperature response for all PBZT/

Sn ceramic samples is linear and can be explained by a thermally activated transport process of Arrhenius type [34]. Due to the creation of defects, as well as vacancies at high temperature, significant differences in conductivity at lower and high temperatures are observed. With a rise in temperature, the reduction of grain boundary resistance results in the lowering of the barrier for the mobility of charge carriers participating in grain boundary conduction.

3.4 Dielectric and relaxor ferroelectric properties

Figure 5 shows temperature dependencies of dielectric constant for the PBZT/Sn ceramics. Tin isovalent doping causes a decrease of phase transition temperature in the PBZT/Sn material. It was detected that T_m shifted toward lower temperature with increasing SnO_2 contents (Fig. 5, Table 1), which might be attributed to decreased internal stress in the structure [35]. The ability to manipulate the temperature of the phase transition of the ceramic material through doping allows to eliminate the problem associated with a change in the usable properties of the material (i.e. energy activation of conductivity, coefficient of thermal expansion), which is important for application-related reasons.
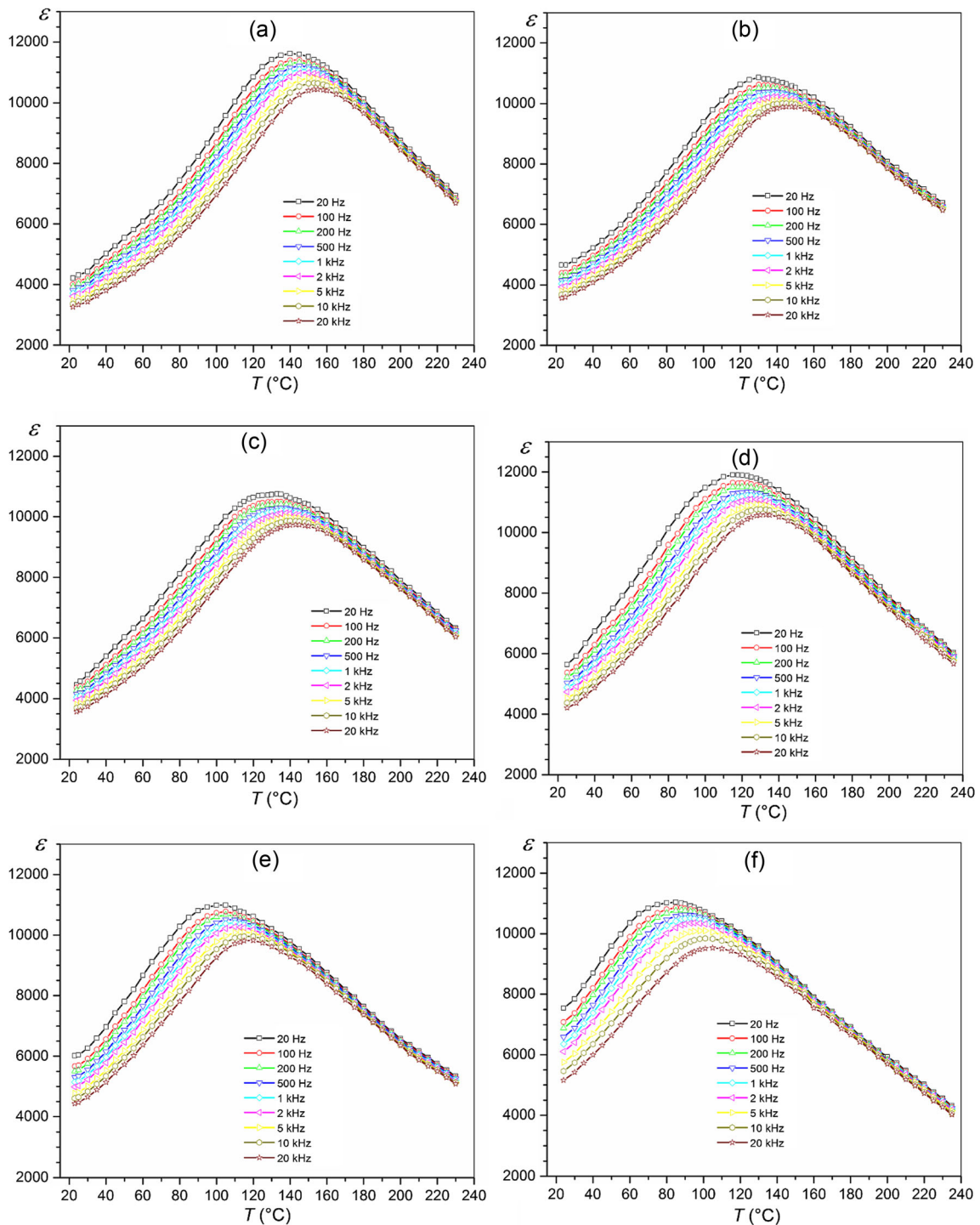
Temperature dependences of dielectric constant of the PBZT/Sn have broad character of ferroelectric-paraelectric phase transition (Fig. 5) – as for many other relaxor materials. Additionally, the tin admixture decreases the maximum of dielectric constant at T_m temperature. Comparing dielectric properties of obtained PBZT/Sn with ceramics obtained at higher sintering temperature and longer time [28], all investigated samples exhibit higher values of dielectric constants at RT as well as at T_m temperature. Also, the phase transition from the ferroelectric to paraelectric phase takes place in a narrower temperature range for the PBZT/Sn ceramic samples investigated in the present paper.

At RT, with the increase of tin admixture in based composition, an increase in values of dielectric constant is observed (Table 1).

In order to evaluate the phase transition we used the modified Curie–Weiss law (3) [36].

$$\frac{1}{\varepsilon} - \frac{1}{\varepsilon m} = C(T - T_m)^{\alpha} \tag{3}$$

where: ε_m is the maximum value of dielectric constant, T_m the temperature of maximum value of dielectric permittivity, C represents Curie–Weiss parameter and α is the parameters indicating the degree of blur of the phase

Fig. 5 Variation of dielectric constant of the PBZT/Sn materials with temperature: (**a**) P-1, (**b**) P-2, (**c**) P-3, (**d**) P-4, (**e**) P-5, (**f**) P-6 (heating cycle)

transition. When $\alpha = 1$ indicates normal Curie-Weiss behavior, while $\alpha = 2$ represents a relaxor phase transition. The α parameter can be calculated by the slope of graph plotted between $\ln(1/\varepsilon - 1/\varepsilon_m)$ and $\ln(T - T_m)$ under 100 Hz (Fig. 6) [37].

A linear fitting was performed and the obtained values are presented in Table 3. The calculated α parameter for ceramic samples indicated ferroelectric relaxation behavior (the samples present a relaxor behavior). It was attributed to Sn^{4+} impregnated into the lattice to replace $Ti^{4+}/$
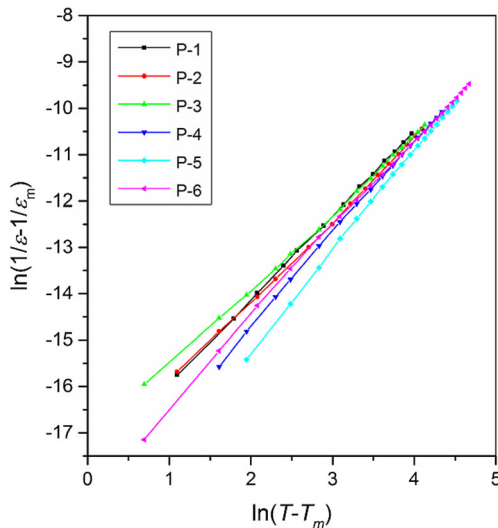
Fig. 6 Plots of $\ln(1/\varepsilon - 1/\varepsilon_m)$ vs. $\ln(T - T_m)$ at temperatures higher than T_m of the PBZT/Sn ceramics (1 kHz)

Zr^{4+}, leading to local compositional fluctuation and the formed polar nano-regions with different temperatures of the phase transition [38].

Dielectric measurements have shown that all PBZT/Sn materials have a wide frequency dispersion of dielectric constant (typical for relaxor materials) and high values of dielectric constant, both at *RT* and at the phase transition temperature (T_m). As the frequency increases, the temperature T_m shifts towards higher temperatures, with a simultaneous reduction of the dielectric constant value. With an increase of the addition of Sn^{4+}, the frequency dispersion is greater (Fig. 5). In the frequency range from 0.02 kHz to 20 kHz for the P-1 sample (without Sn^{4+} admixture), the width of the dispersion range is the smallest (15.2 °C), while for the composition with the highest concentration

of tin (P-6 sample), the width of the dispersion range increases to 26.2 °C.

The frequency dependence of the temperature of maximum permittivity, T_m, in relaxors can be described by the Vogel-Fulcher law (4) which provides some insights into the dynamics of dielectric relaxation [39–41].

$$f_m = f_0 \cdot e^{-\frac{E_a/k}{(T_m - T_{VF})}} \tag{4}$$

where f_m - frequency at which temperature of maximum is equal to T_m, f_0 – pre-exponential factor, E_a - activation energy of local polarization fluctuations for Vogel-Fulcher relation, T_m - temperature of maximum, T_{VF} - so called Vogel-Fulcher temperature below which the freezing process take place, k – Boltzmann constant.

The dielectric measurements show that for the PBZT/Sn ceramics, the temperature of the maximum dielectric constant fulfills the Vogel-Fulcher law. The obtained f_m relationships for PBZT/Sn samples with different tin contents are shown in Fig. 7a, whereas a graph in logarithmic form $\ln f = f(1000/T)$ in Fig. 7b – a dependency that makes it easy to find parameters in the Vogel-Fulcher equation. With increasing of the Sn^{4+} amount (with a smaller ion radius), the VF curves are shifted to lower temperatures, and the possibility of obtaining T_m values at low frequencies increases. This can be attributed to the fact that in the case of low frequencies testes the data are usually noisy [39].

The obtained results adjusted to the experimental results (according to the Eq. 4) are summarized in Table 4, while Fig. 8 shows the dependencies of f_0, T_{VF} and E_a parameters on the content of tin (*a*) with fitting results. Within the fitting results, it is clearly seen that with an increase in Sn^{4+} content, the pre-exponential factor, f_0, and freezing temperature, T_{VF}, decrease systematically. In case of the activation energy, E_a, it initially decreases with an increase in Sn^{4+} content, and successively it becomes almost constant (for samples from P-3 to P-6), as was observed. Dependency of the $f_0(a)$ can be described by equation:

$$f_0(a) = f_0(0) + A_1 \cdot e^{-\frac{a}{B_1}} \tag{5}$$

with parameters $f_0(0) = 0$ Hz, $A_1 = 2.155 \times 10^9$ Hz, $B_1 = 0.029$. Dependency of the $T_{VF}(a)$ can be described by equation:

$$T_{VF}(a) = T_{VF}(0) + A_2 \cdot e^{-\frac{a}{B_2}} \tag{6}$$

with parameters $T_{VF}(0) = -130$ K, $A_2 = 1.31 \times 10^5$ K, $B_2 = 264.6$. Dependency of the $E_a(a)$ can be described by equation:

$$E_a(a) = E_a(0) + A_3 \cdot e^{-\frac{a}{B_3}} \tag{7}$$

with parameters $E_a(0) = 0.0298$ eV, $A_3 = 0.0141$ eV, $B_3 = 0.050$.

Table 3 Parameters of the PBZT/Sn ceramics obtained from Curie–Weiss law

	T_m (°C)	T_{CW} (°C)	T_B (°C)	ΔT_m (°C)	α
P-1	147	51	180	33	1.817
P-2	140	5	185	45	1.757
P-3	138	14	184	46	1.723
P-4	123	69	183	60	1.952
P-5	108	44	167	61	1.985
P-6	93	40	162	69	1.881

T_m - temperature as the appeared maximum of dielectric constant; T_B - the temperature when the permittivity starts to follow the Curie–Weiss law, ΔT_m - the temperature deviation that reveals the level of dielectric diffusion, α is the parameters indicating the degree of blur of the phase transition

Fig. 7 The $f_m(T_m)$ relationships (**a**) and $\ln f = f(1000/T)$ (**b**) for PBZT/Sn ceramics. Solid lines - the result of fitting based on the Eq. (4)
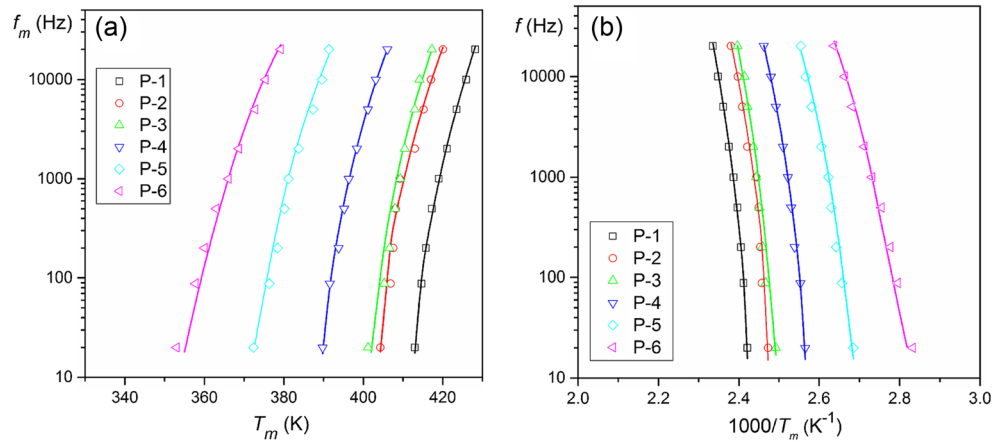
The addition of tin in the base composition also has a significant effect on the value of the dielectric loss of PBZT/Sn ceramics (Fig. 9). For all compositions at *RT*, dielectric loss remains at a low level (for 1 kHz). At the temperature of the phase transition, the value of dielectric loss, with the increase in the amount of tin added to the basic ceramic composition, increases (Table 1). Also at temperature dependences $\tan\delta(T)$, dielectric loss increases over the entire measuring area, with increasing frequency of the measuring field. For all PBZT/Sn samples above, the phase transition temperature the values of dielectric loss are significantly reduced for all measuring frequencies. The observed mechanism in this range can be associated with many phenomena, e.g. the disappearance of domains at T_m temperature abruptly reduces the dielectric loss or an increase of the ac conductivity that increases loss tangent with the increase in temperature [42]. Comparing the obtained PBZT/Sn ceramics with the ones obtained in [28], we can say that all ceramic samples show slightly higher values of dielectric loss in higher frequency.

**Table 4** Summary of the Vogel–Fulcher fitting parameters of the PBZT/Sn ceramics

	f_0 (Hz)	E_a/k (K)	T_{VF} (K)	E_a (eV)
P-1	2.15×10^9	498.2	385.2	0.043
P-2	1.08×10^9	489.7	375.1	0.042
P-3	5.42×10^8	400.8	377.9	0.034
P-4	2.72×10^8	380.6	366.0	0.033
P-5	1.36×10^8	379.0	349.0	0.033
P-6	6.85×10^7	378.7	332.6	0.033

f_0 – pre-exponential factor; E_a - activation energy for Vogel-Fulcher relation, T_{VF} - Vogel-Fulcher temperature below which the freezing process take place, k – Boltzmann constant

3.5 Ferroelectric properties

Hysteresis loops at various temperatures for the PBZT/Sn ceramics for 1 Hz are presented in Fig. 10. At 30 °C, for all ceramic samples (except P-6 sample) the hysteresis loops are well saturated with high values of spontaneous polarization, P_S and remnant polarization, P_R. With increasing amount of tin in PBZT/Sn, the values of the P_R remnant polarization decreases from 19.88 μC/cm (for P-1) to 7.28 μC/cm (for P-6 sample). In the same conditions, the highest values of the E_C coercive field is 0.58 kV/mm for the P-1 sample (without tin doped). Tin isovalent doping of the PBZT material causes a decrease of coercive field, which can be related to effect of domain wall pining with little dipole defects in the structure [43]. Decrease of the value of the P_R can be attributed to the decrease of BO_6 octahedrons, as a result of the substitution of smaller Sn^{4+} ions into B positions of the perovskite structure. In case of the P-6 sample, the differences in P_R and E_C values can be associated with the inter-space size of octahedron, as well as the values of internal stress related with the excess of Sn^{4+} content, or a weak clampping effect of domain walls with bigger grain sizes [43].

The increase in the frequency of the measuring field slightly expands the hysteresis loop and reduces values of the remnant polarization (selected enlarged region in Figs 10 inside). For samples with low tin contents, together with increase of measurement field frequency, the coercive field increases stronger than for the samples with higher amount of tin. This may be related to the appearance of relaxor properties with increasing the amount of tin admixture in the PBZT/Sn compound. With increasing temperature, the hysteresis loops become narrower (Fig. 10). For all samples with increasing temperature the coercive fields decrease and in this
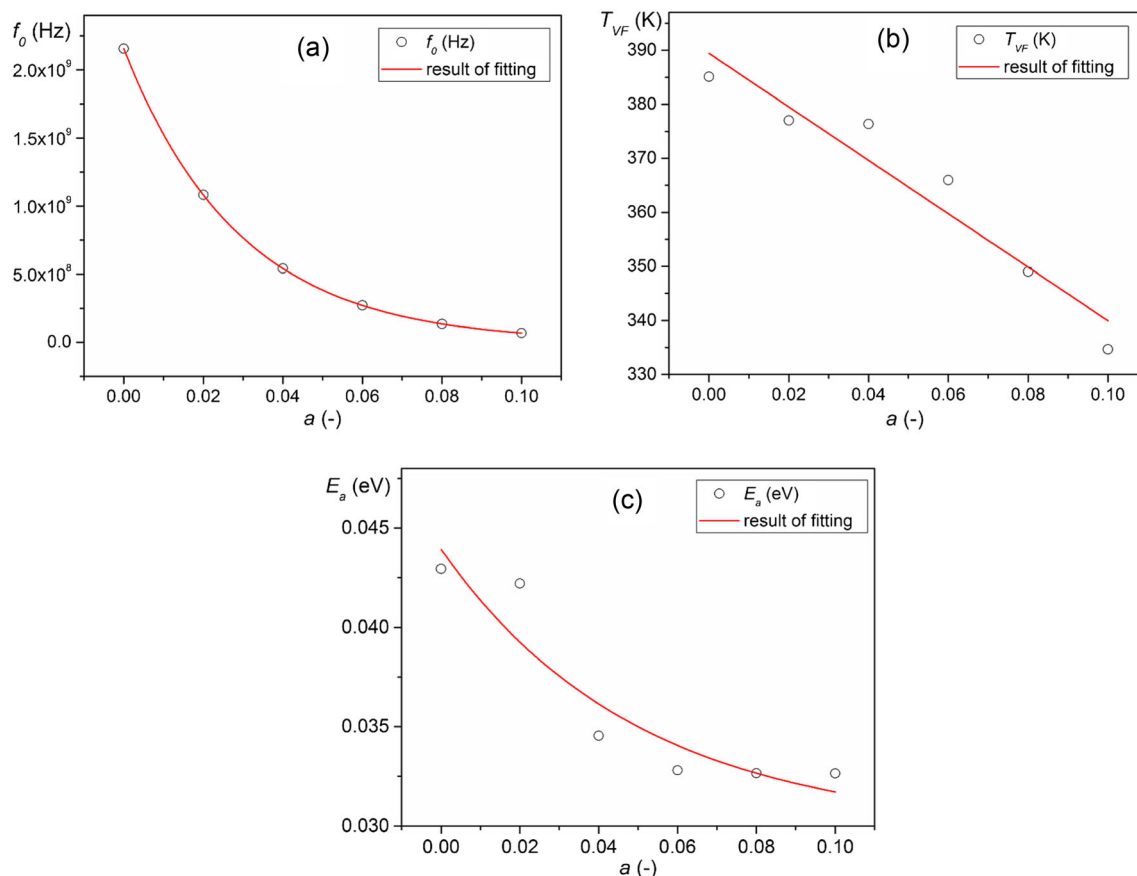
Fig. 8 The dependencies of parameters f_0, T_{VF} and E_a on the content of tin for PBZT/Sn ceramics

same time the values of P_R remnant polarization decrease. Comparing results of ferroelectric measurements of the PBZT/Sn ceramics obtained at higher temperatures and longer time [28], we can conclude that the values of remnant polarization P_R and coercive field E_C are higher.

Rectangularity coefficient of the hysieresis loop was calculated from the following formula (8):

$$a_{rec} = \frac{P_R}{P_{max}} \qquad (8)$$

where a_{rec} - rectangularity coefficient, P_R - remnant polarization, P_{max} - maximum value of polarization. The rectangularity coefficient a_{rec} decreases with the increasing amount of tin in PBZT/Sn composition (Table 1).

The dependency of P_R remnant polarization and E_C coercive field on tin content at different temperatures are presented in Fig. 11. For all PBZT/Sn samples, with the temperature rise, there is a trend of decreasing P_R and E_C parameters.

3.6 Electromechanical properties

Figure 12 shows the results of electromechanical investigations at *RT* for all obtained ceramics obtained at a frequency of 1 Hz. It is commonly known, the electric field induced strain in ceramic sample is caused by the domain switching, number of polarization states, electrostriction and the applied electric field [44]. The change in the character of strain mechanism may be seen with increasing tin content. In samples with small tin content, the strain v.s. the electric field is typical for piezoelectric materials (linear *S-E* dependency). For high amounts of Sn^{4+} in PBZT/Sn composition, the loops become typical for relaxor materials (the strain is proportional to the second power of the electric field).

In an ideal defect free single crystal that is poled perfectly, the remnant strain is represented by its lattice distortion [45]. The electric-field-induced strain in ceramic material is caused by domain switching, number of polarization states, electrostriction and the applied electric field [44]. In case of the P-1 sample (without tin doped), the remnant strain is the highest (0.131%). With an increase
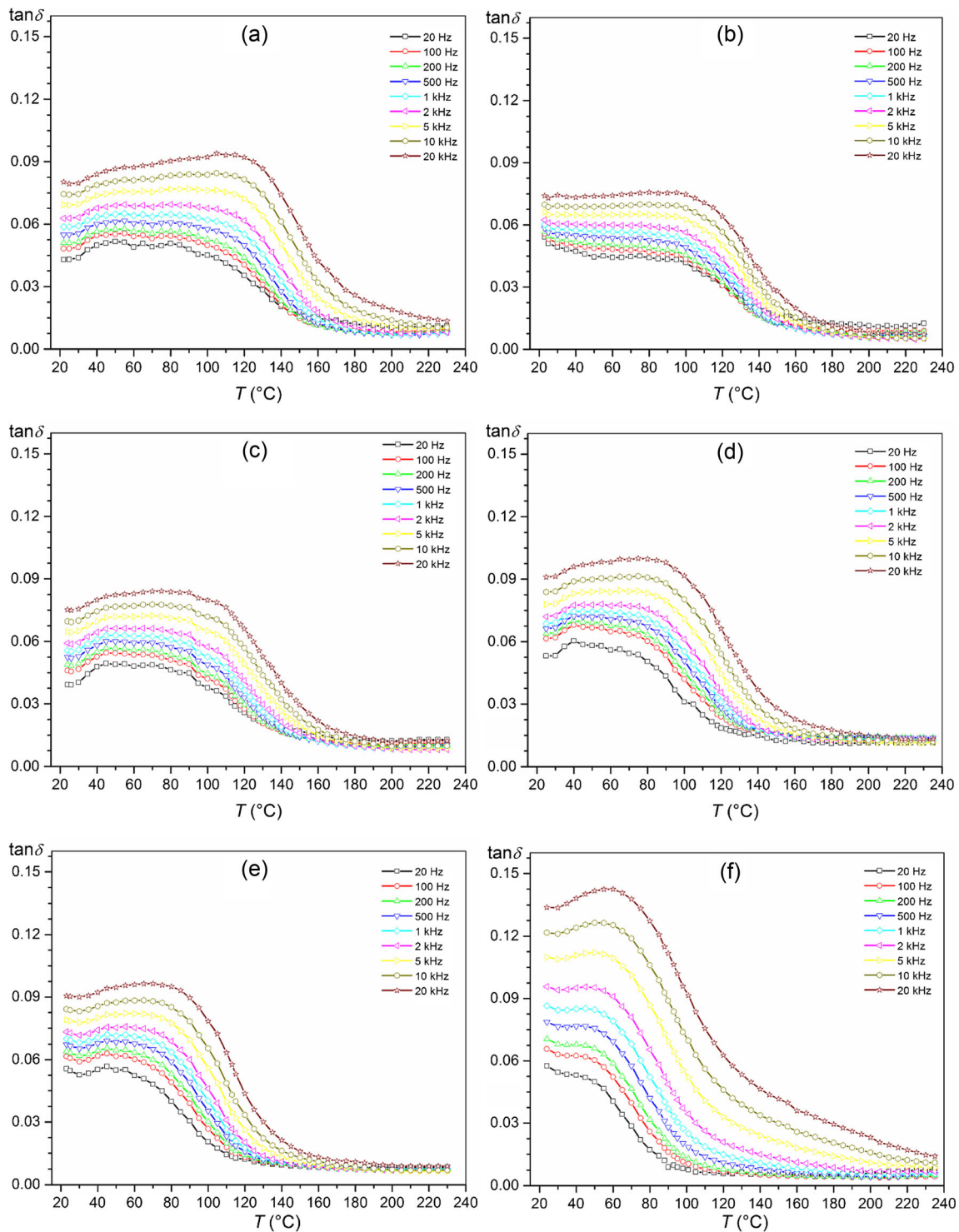
Fig. 9 Variation of dielectric loss of the PBZT/Sn materials with temperature: (**a**) P-1, (**b**) P-2, (**c**) P-3, (**d**) P-4, (**e**) P-5, (**f**) P-6 (heating cycle)

in admixture of tin in PBZT material, the values of remnant strain decreased and were 0.076%, 0.047%, 0.038%, 0.015 and 0.007% for P-2, P-3, P4, P5 and P-6 samples, respectively. This diminishing trend can be attributed to the accumulation of various reasons, such as randomness of grain orientations which naturally confine the orientation of domains, depolarization fields arising from defects, pinning of domains, etc. [45].
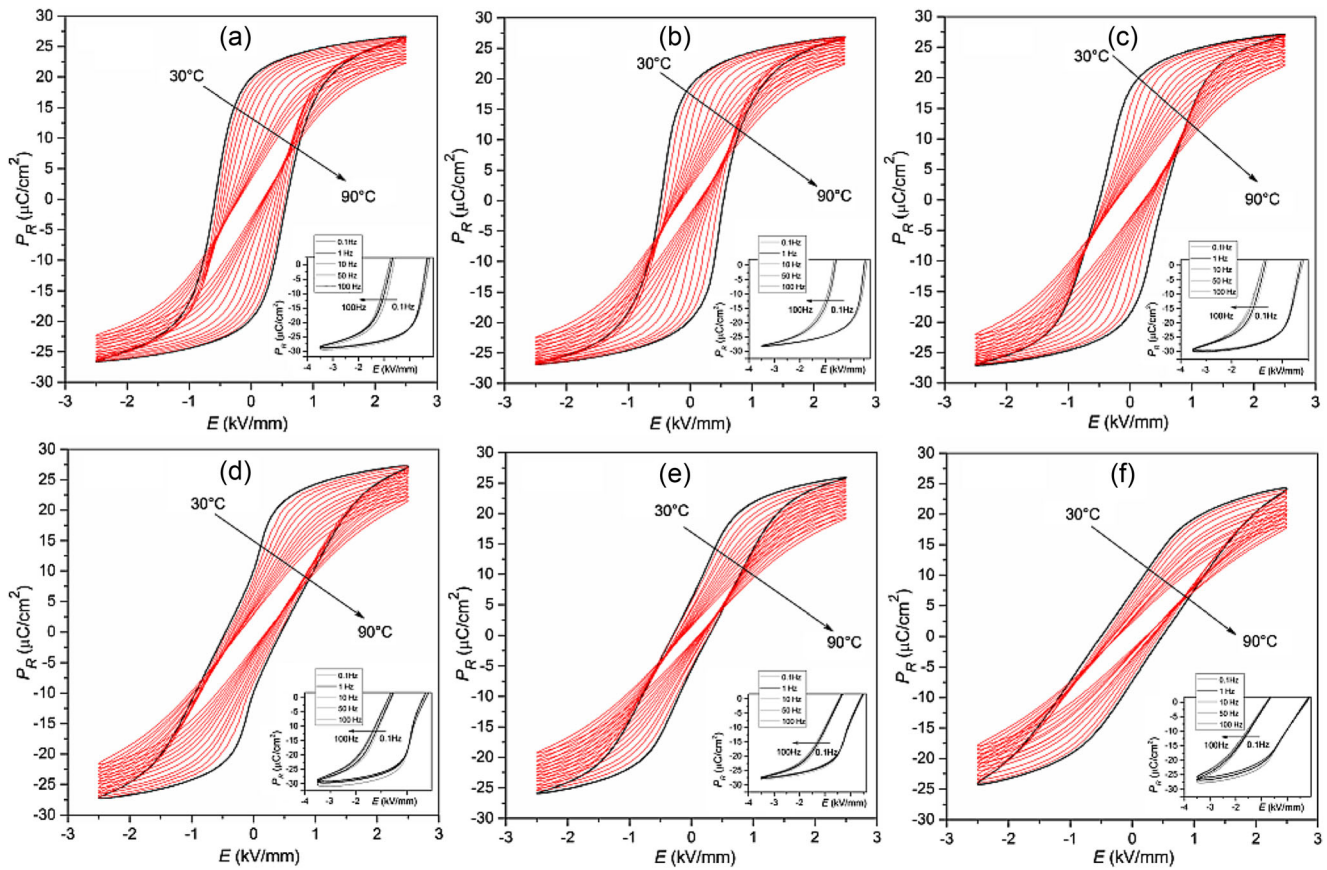
Fig. 10 Variation of P-E hysteresis loops of the PBZT/Sn materials with temperature (f = 1 Hz): (**a**) P-1, (**b**) P-2, c) P-3, d) P-4, e) P-5, f) P-6; (inside: selected enlarged region P-E hysteresis loops for the different frequencies and at RT)

In piezoelectric applications (for example, in transducers or actuators), the large signal piezoelectric coefficient, d_{33}^* is one of critical parameters and can be calculated by the following formula [46]:

$$d_{33}^* = \frac{S_{max}}{E_{max}} \tag{9}$$

where S_{max} is the maximum induced strain at maximum electric field E_{max}. The values of d_{33}^* are from 729 pm/V (for P-1) to 427 pm/V (for P-6) at 3.75 kV/mm (Table 1). Results of similar investigations of d_{33}^* have been made in papers [45, 46]. In our material it can be interpreted as negative strain decreased with increasing SnO_2 content. However during this (i.e. with Sn^{4+} content increase) we

Fig. 11 The dependency of the (**a**) remnant polarization P_R and (**b**) coercive field E_C on tin content of the PBZT/Sn ceramics (frequency 1 Hz, RT)
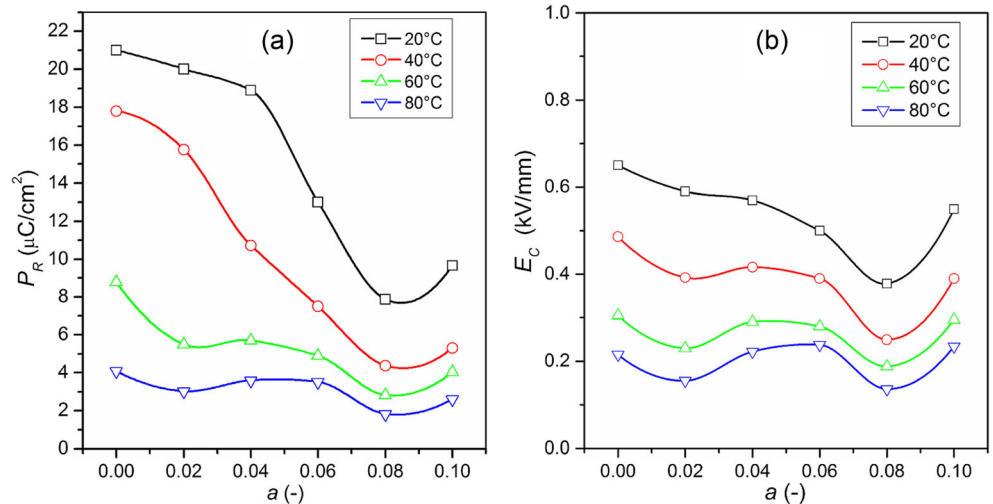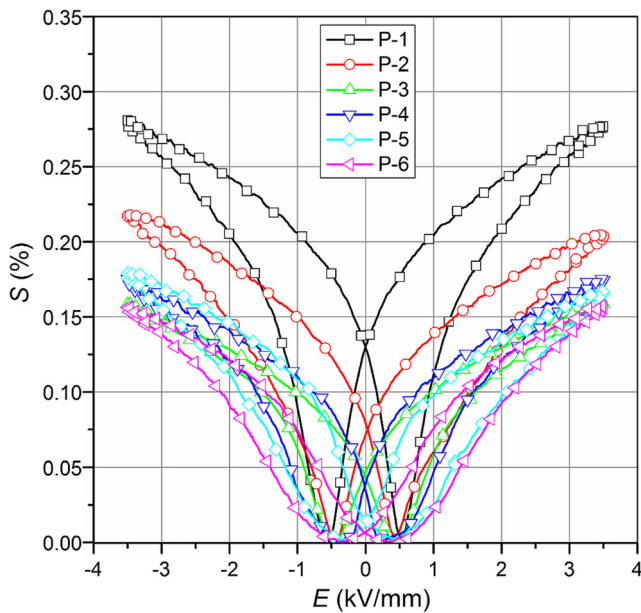
Fig. 12 Strain vs. electric field of the PBZT/Sn ceramics

can also see the change of *S-E* loop during that. It can be important for applications in which we need *S-E* loops typical for relaxor materials such as electrostrictive transducers. Comparing with PBZT/Sn ceramics obtained using technological conditions like in [28] ceramic samples show higher values of mechanical strain.

4 Conclusion

In the present work, six PBZT/Sn ceramic compositions with different amounts of Sn^{4+} (*a* from the range 0.0 to 0.1) sintered at 1250 °C/4 h, were obtained. The results show that all of the ceramic samples are well sintered and the grain boundaries are clear with few pores. The increase of the amount of tin admixture in the basic composition of PBZT increases the average size of grains. The PBZT/Sn ceramic samples exhibit high values of dielectric permittivity at the phase transition temperature. Increasing the amount of tin admixture also results in a shift of the ferroelectric phase transition towards lower temperatures and at the same time reduces the maximum of dielectric permittivity at T_C temperature. The ability to manipulate the temperature of the phase transition of the PBZT ceramic material through doping allows to eliminate the problem associated with the change in the usable properties of the material, which is important due to applications. Excessive SnO_2 contents doping of the PBZT materials might give rise to the structure defect and lattice stress, which leaded to deteriorated dielectric and ferroelectric properties of the ceramics.

The measurements performed exhibit that the introduction of SnO_2 to the base PBZT composition positively influences the microstructure and electrical properties of the ceramics

(especially on the parameters essential for practical applications, from the area of micromechatronics and microelectronics). The introduction of the Sn^{4+} ion to the basic PBZT composition also allows to control the shape of the dielectric hysteresis loop and the strain loop.

References

1. G. Vats, R. Vaish, Piezoelectric material selection for transducers under fuzzy environment. J. Adv. Ceram. **2**(2), 141–148 (2013)
2. H. Zhang, S. Jiang, J. Xiao, K. Kajiyoshi, Piezoelectric and dielectric aging of $Bi_{0.5}(Na_{0.82}K_{0.18})_{0.5}TiO_3$ lead-free ferroelectric thick films. J. Appl. Phys. **107**(12), 124118 (2010)
3. H. Zhang, S. Jiang, Y. Zeng, B site doping effect on depinning in $Pb(Mn_{1/3}Nb_{1/3}Sb_{1/3})_x(Zr_{0.825}Ti_{0.175})_{1-x}O_3$ ferroelectric ceramics. Appl. Phys. Lett. **93**(19), 192901 (2008a)
4. L.I. Gurskii, J. Macutkevic, J. Banys, A. Poddubskaya, M.N. Saraseko, A.V. Petrov, N.A. Kalanda, N.A. Sobolev, Synthesis and dielectric properties of $Pb_{0.85}Ba_{0.25}Zr_{0.53}Ti_{0.47}O_3$ compounds with nano-inclusions of cu and Ni. Phys. Status Solidi C **10**(4), 640–645 (2013)
5. N. Zhang, Z. Xu, Y. Feng, X. Yao, Dielectric and relaxor ferroelectric properties of Ba-doped $Pb(Zr,Ti)O_3$ ceramics. J. Electroceram. **21**(1-4), 609–612 (2008b)
6. G. Li, G.H. Haertling, Dielectric, ferroelectric and electric field induced strain properties of $(Pb_{1-x}Ba_x)(Zr_{1-y}Ti_y)O_3$ ceramics. Ferroelectrics **166**(1), 31–45 (1995)
7. D. Bochenek, R. Skulski, P. Wawrzała, D. Brzezińska, Dielectric properties of $Pb_{0.75}Ba_{0.25}(Zr_{0.65}Ti_{0.35})_{1-z}Sn_zO_3$ ceramics. Ferroelectrics **418**(1), 82–87 (2011)
8. M. Lines, A. Glass, *Principles and Applications of Ferroelectrics and Related Materials* (Oxford University Press, Oxford, 2000)
9. N. Texier, C. Courtois, M. Teaianidis, A. Leriche, Powder process influence on the characteristics of Mn, W, Sb, Ni-doped PZT. J. Eur. Ceram. Soc. **21**(10-11), 1499–1502 (2001)
10. M.R. Soares, A.M.R. Senos, P.Q. Mantas, Phase coexistence region and dielectric properties of PZT ceramics. J. Eur. Ceram. Soc. **20**(3), 321–334 (2000)
11. J. Suchanicz, N.-T. Kim-Ngan, K. Konieczny, I. Jankowska-Sumara, A.G. Balogh, Soft and hybrid-doped $Pb(Zr,Ti)O_3$ ceramics under stress, electric field, and temperature loading. J. Appl. Phys. **109**, 104105 (2011)
12. P.K. Panda, B. Sahoo, S. Raja, M.P. Vijaya Kumar, V. Shankar, Electromechanical and dynamic characterization of in-house-fabricated amplified piezo actuator. Smart Materials Research **2012**, 203625 (2012)
13. M. Venkata Ramana, S. Roopas Kiran, N. Ramamanohar Reddy, K.V. Siva Kumar, V.R.K. Murthy, B.S. Murty, Investigation and characterization of $Pb(Zr_{0.52}Ti_{0.48})O_3$ nanocrystalline ferroelectric

ceramics: By conventional and microwave sintering methods. Mater. Chem. Phys. **126**(1-2), 295–300 (2011)

14. T. Ikeda, Studies on (BaPb)(TiZr)O$_3$ system. J. Phys. Soc. Japan. **14**(2), 168–174 (1959)

15. Y. Xu, *Ferroelectric Materials and their Applications* (Elsevier, North Holland, NY, USA, 1991)

16. J. Bartkowska, J. Ilczuk, The internal friction and the relaxation time spectrum of ferroelectric ceramic PZT type. Acta Phys. Pol. A **114**(6A), A7 (2008)

17. P. Liu, X. Yao, Dielectric properties and phase transitions of (Pb$_{0.87}$La$_{0.02}$Ba$_{0.1}$) (Zr$_{0.6}$Sn$_{0.4}$K$_x$Ti$_x$)O$_3$ ceramics with compositions near AFE/RFE phase boundary. Solid State Commun. **132**(12), 809–813 (2004)

18. J. Hańderek, M. Adamczyk, Z. Ujma, Dielectric and pyroelectric properties of (Pb$_{1-x}$Ba$_x$)(Zr$_{0.70}$Ti$_{0.30}$)O$_3$ [x=0.25÷0.35] ceramics exhibiting relaxor ferroelectrics behavior. Ferroelectrics **233**, 253 (1999)

19. M. Adamczyk, Z. Ujma, J. Hańderek, Relaxor behavior of La-modified (Pb$_{0.75}$Ba$_{0.25}$)(Zr$_{0.70}$Ti$_{0.30}$)O$_3$ ceramics. J. Appl. Phys. **89**(1), 542–547 (2001)

20. K.H. Yoon, Y.W. Kim, D.H. Kang, Donor substitution effect on dielectric and electrostrictive properties of (Pb$_{0.73}$Ba$_{0.27}$)(Zr$_{0.75}$Ti$_{0.25}$)O$_3$ ceramics. J. Mater. Sci. Lett. **17**, 159 (1998)

21. M.-J. Pan, R.J. Rayne, B.A. Bender, Dielectric properties of niobium and lanthanum doped lead barium zirconate titanate relaxor ferroelectrics. J. Electroceram. **14**(2), 139–148 (2005)

22. M.H. Lente, E.N. Moreira, D. Garcia, J.A. Eiras, P.P. Neves, A.C. Doriguetto, V.R. Mastelaro, Y.P. Mascarenhas, Induction of relaxor state in ordinary ferroelectrics by isovalent ion substitution: A pretransitional martensitic texture case. Phys. Rev. B **73**(5), 054106 (2006)

23. K. Uchino, Electrostrictive actuators: Materials and application. Bull. Amer. Ceram. Soc. **65**, 647 (1986)

24. C.G. O'Neill, C.H. O'Neill, Ferroelectric actuators in the electromechanical interface. Opt. Eng. **29**(11), 1383 (1990)

25. R. Zachariasz, D. Bochenek, Properties of the PZT type ceramics admixed with barium and niobium. Arch. Metall. Mater. 54, 4, 895 (2009)

26. P.K. Panda, B. Sahoo, PZT to lead free piezo ceramics: A review. Ferroelectrics **474**(1), 128–143 (2015)

27. J. Rödel, W.J. Klaus, T.P. Seifert, E.-M. Anton, T. Granzow, D. Damjanovic, Perspective on the development of lead-free piezoceramics. J. Am. Ceram. Soc. **92**(6), 1153–1177 (2009)

28. R. Skulski, D. Bochenek, P. Wawrzała, G. Dercz, D. Brzezińska, Technology and properties of PBZTS ceramics. Int. J. Appl. Ceram. Technol. **10**(2), 330–338 (2013)

29. M. Mir, V.R. Mastelaro, P.P. Neves, A.C. Doriguetto, D. Garcia, M.H. Lente, J.A. Eiras, Y.P. Mascarenhas, X-ray powder diffraction structural characterization of Pb$_{1-x}$Ba$_x$Zr$_{0.65}$Ti$_{0.35}$O$_3$ ceramic. Acta Cryst **63**, 13 (2007)

30. W. Travis, E.N.K. Glover, H. Bronstein, D.O. Scanlon, R.G. Palgrave, On the application of the tolerance factor to inorganic and hybrid halide perovskites: A revised system. Chem. Sci. **7**(7), 4548–4556 (2016)

31. S.F. Hoefler, G. Trimmel, T. Rath, Progress on lead-free metal halide perovskites for photovoltaic applications: A review. Monatsh. Chem. **148**(5), 795–826 (2017)

32. L. Dong, D.S. Stone, R.S. Lakes, Enhanced dielectric and piezoelectric properties of xBaZrO$_3$–(1-x)BaTiO$_3$ ceramics. J. Appl. Phys. **111**(8), 084107 (2012)

33. O. Raymond, R. Font, N. Suárez-Almodovar, J. Portelles, J.M. Siqueiros, Frequency-temperature response of ferroelectromagnetic PbFe$_{1/2}$Nb$_{1/2}$O$_3$ ceramics obtained by different precursors. Part I. Structural and thermo-electrical characterization. J. Appl. Phys. **97**(8), 084107 (2005)

34. S.O. Kasap, *Principles of Electronic Materials and Devices, 2nd Edn* (McGraw-Hill, Boston, 2002)

35. C. Mao, S. Yan, S. Cao, C. Yao, F. Cao, G. Wang, X. Dong, X. Hu, C. Yang, Effect of grain size on phase transition, dielectric and pyroelectric properties of BST ceramics. J. Eur. Ceram. Soc. **34**(12), 2933–2939 (2014)

36. D. Bochenek, Z. Surowiak, J. Krok-Kowalski, J. Poltierova-Vejpravova, Influence of the sintering conditions on the physical proprieties of the ceramic PFN multiferroics. J. Electroceram. **25**(2-4), 122–129 (2010)

37. O. Raymond, R. Font, N. Suárez, J. Portelles, J.M. Siqueiros, Effects of two kinds of FeNbO$_4$ precursors in the obtainment and dielectric properties of PFN ceramics. Ferroelectrics **294**, 141 (2003)

38. X.L. Chao, Z.M. Wang, Y. Tian, Y.Z. Zhou, Z.P. Yang, Ba(Cu$_{0.5}$W$_{0.5}$)O$_3$ – Induced sinterability, electrical and mechanical properties of (Ba$_{0.85}$Ca$_{0.15}$Ti$_{0.90}$Zr$_{0.10}$)O$_3$ ceramics sintered at low temperature. Mater. Res. Bull. **66**, 16–25 (2015)

39. A. Rotaru, F.D. Morrison, Vogel–Fulcher analysis of relaxor dielectrics with the tetragonal tungsten bronze structure: Ba$_6$MNb$_9$O$_{30}$ (M = Ga, Sc, in). J. Therm. Anal. Calorim. **120**(2), 1249–1259 (2015)

40. H.N. Tailor, A.A. Bokov, Z.-G. Ye, Dielectric characterization of (1-x)PMN–xPT (x = 0.07 and 0.10) ceramics synthesized by an ethylene glycol-based soft chemical route. IEEE Trans. Ultrason. Ferroelectr. Freq. Control **58**(9), 1920–1927 (2011)

41. T. Maiti, R. Guo, A.S. Bhalla, Structure-property phase diagram of BaZr$_x$Ti$_{1-x}$O$_3$ system. J. Am. Ceram. Soc. **91**(6), 1769–1780 (2008)

42. S.B. Majumder, S. Bhattacharyya, R.S. Katiyar, A. Manivannan, P. Dutta, M.S. Seehra, Dielectric and magnetic properties of sol-gel-derived lead iron niobate ceramics. J. Appl. Phys. **99**(2), 024108 (2006)

43. Y. Tian, S. Li, Y. Gong, Y. Yum, Y. Tang, P. Liu, Q. Jing, Diversified electrical properties of Ba$_{0.90}$Ca$_{0.10}$Ti$_{0.95}$Zr$_{0.05}$O$_3$–xRuO$_2$ ceramics with defect electron complexes. Mater. Chem. Phys. **204**, 163 (2018)

44. A.S. Karapuzha, N.K. James, H. Khanbareh, S. van der Zwaag, W.A. Groen, Structure, dielectric and piezoelectric properties of donor doped PZT ceramics across the phase diagram. Ferroelectrics **504**(1), 160–171 (2016)

45. W. Jo, R. Dittmer, M. Acosta, J. Zang, C. Groh, E. Sapper, K. Wang, J. Rödel, Giant electric-field-induced strains in lead-free ceramics for actuator applications–status and perspective. J. Electroceram. **29**(1), 71–93 (2012)

46. H. Zhang, P. Xu, E. Patterson, J. Zang, S. Jiang, J. Rödel, Preparation and enhanced electrical properties of grain-oriented (Bi$_{1/2}$Na$_{1/2}$)TiO$_3$-based lead-free incipient piezoceramics. J. Eur. Ceram. Soc. **35**(9), 2501–2512 (2015)